Thermochimica Acta 500 (2010) 100–105

Contents lists available at ScienceDirect

Thermochimica Acta

journal homepage: www.elsevier.com/locate/tca

Application of a deconvolution method to construct aqueous phase diagram

R.C. Gosh, S. Tanaka, A. Toda*

Graduate School of Integrated Arts and Sciences, Hiroshima University, 1-7-1 Kagamiyama, Higashi-Hiroshima 739-8521, Japan

ARTICLE INFO

Article history:
Received 14 September 2009
Received in revised form
27 December 2009
Accepted 4 January 2010
Available online 14 January 2010

Keywords:
DSC
Calibration
Instrumental coefficient
Aqueous solution
Phase diagram

ABSTRACT

Signals obtained from a differential scanning calorimeter (DSC) include instrumental effects of time lag due to slow thermal conductance. The dynamic response of samples is influenced by the effects, especially on the occasion of phase transitions. A deconvolution method calibrating the instrumental effects for the heat-flux DSC is reviewed and applied to the eutectic mixtures of aqueous solutions of NaCl and glycerol to determine the phase behaviors without ambiguity in the interpretation of the peak profile. The method is useful for the measurements with fast heating runs, which inevitably have larger time lag but is required for *e.g.* polymeric systems to reduce reorganization on heating. The results of the deconvolution are well agreed with the data in the literature.

1. Introduction

A conventional differential scanning calorimetry of heat flux type (CDSC-HF) measures the temperature of a sample and the heat flow rate from the sample. This tool has been widely used to study the heat absorption or release in physical, chemical and biological processes [1–3]. Among them, the study of phase behavior has been utilizing CDSC-HF as a source of fundamental information of the phenomena [1]. Phase diagrams provide us information about a phase at a given temperature (T) and composition (x) of the system of interest. Unfortunately, however, DSC apparatuses give us a distorted signal of the heat flow rate, as shown in a schematic representation (Fig. 1). The schematic phase diagram of a eutectic mixture shown in Fig. 1(a) predicts an ideal heat flow rate-temperature diagram (thermogram) shown by a solid curve in Fig. 1(b) at a prepared composition, x_1. In reality, however, the thermogram is distorted like the one shown by a dashed curve in Fig. 1. The distortion of the thermogram in Fig. 1(b) clearly requires careful consideration to the peak profile of CDSC-HF data in order to construct the correct phase diagram.

In the standard interpretation of the peak profile of heating runs, the sample temperature is supposed to be kept constant at the eutectic point when the temperature reaches at the lower temperature peak. Hence the distortion on the peak profile at the eutectic point can be calibrated by the extrapolation of the peak to the onset temperature. On the other hand, the higher temperature peak should end ideally at the liquidus point at the prepared composition x_1. The ending of the peak, however, is always distorted by a time lag between the end of the melting and the return of the heating rate to the programmed one. Therefore, the extrapolated ending temperature or the second peak temperature does not necessarily correspond to the true liquidus point. The detailed information of the instrument is required for the accurate determination of the liquidus point, which in turn is essential to construct the correct phase diagram. To deconvolute the instrumental effects from the raw data, it is important to know the exact reasons of the distortion.

Instrumental effect such as time or temperature lag is not a new issue. Regarding this, there have been several methods based on mathematical treatments [4–8] and extrapolations [9,10] proposed in the last four decades. Among them, Boettinger et al. [4] recently reviewed thermal lag problems and presented possible mathematical models for both pure metal and eutectic alloys. In their models, importance was given to the sample kinetics (such as solute diffusion in alloys) rather than the instrumental effects caused by the heat transfer between sample and instrument. On the other hand, extrapolation methods [9,10] paid much attention on the choice of the baselines to determine the true melting temperatures, as shown in Fig. 2. The extrapolated peak-onset temperature shown in Fig. 2(a) was assigned as the true melting temperature of the pure material and was determined at the intersection point of the

* Correesponding author: Tel.: +81 82 424 6558; fax: +81 82 424 0757.
E-mail address: atoda@hiroshima-u.ac.jp (A. Toda).

0040-6031/$ – see front matter © 2010 Elsevier B.V. All rights reserved.
doi:10.1016/j.tca.2010.01.004

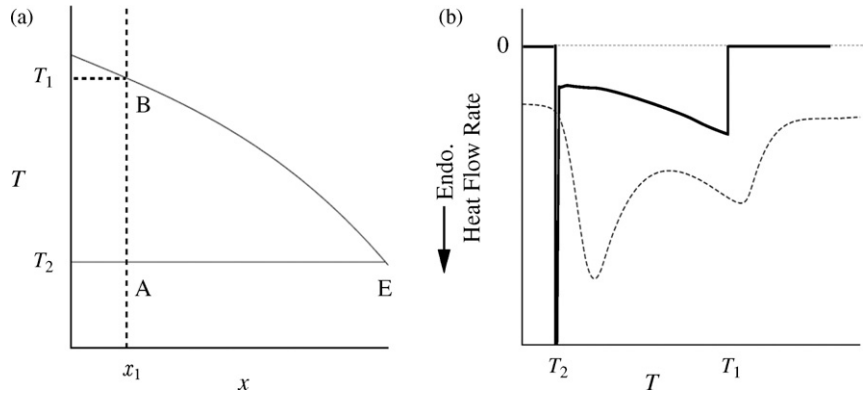

Fig. 1. Schematic representation of (a) a phase diagram of a eutectic mixture and (b) the heat flow rate-temperature diagram (thermogram). In (a), liquidus (BE) and solidus (AE) lines meet at the eutectic point (E). T_2 is the eutectic temperature and T_1 is the ending temperature of melting at the composition x_1 in the eutectic mixture. In (b), the solid curve is an ideal heat flow rate of transition expected from the phase diagram in (a), and the dashed curve is the corresponding one distorted by instrumental effects.

auxiliary line through the descending peak slope with the linearly extrapolated initial baseline in GEFTA [9] method and with the abscissa, *i.e.* the line of zero heat flow rate, in SARGE [10] method, respectively. To determine the melting temperatures of the complex event as shown in Fig. 2(b), the auxiliary line is drawn from the individual peak tips to the baseline at the slope, γ, set at the same slope as that of the melting of pure material, which is supposed to proceed at a fixed constant temperature.

The present paper mainly focuses on the instrumental effects on the melting process of a eutectic mixture, so that the effects are more significant for faster heating runs because of larger instrumental time lag, while the kinetics of melting is supposed to be fast enough. For this reason, we follow the method of Toda et al. [8], who have suggested a calibration method of deconvolution of the instrumental effects to obtain the true sample temperature and heat flow rate from the sample. We have recently applied the method using CDSC-HF on eutectic ternary mixtures in our previous paper [11] without any detailed explanation. Since the mixtures were aqueous solutions of poly(ethylene glycol) with the addition of NaCl, the heating runs at sufficiently high rates were necessary to reduce the reorganization of polymeric crystals. Thus the application of the deconvolution method was essential to construct the phase diagrams accurately. In this paper, we review the calibration method in detail for the study of the phase behavior of eutectic mixtures using CDSC-HF, and examine the applicability using aqueous solutions of NaCl and glycerol, whose phase diagrams are available in the literature. Then, we compare the results of the deconvolution method with those of extrapolation methods [9,10].

2. Model

2.1. The basic equations

Since we use the method proposed by Toda et al. [8] for the study of phase transitions in solution, here we review this method. Following the Mraw's model [5], CDSC-HF is modeled by the following equations describing the heat flow rate in the sample side,

$$C_s \frac{dT_s}{dt} = K_1(T_m - T_s) + F \tag{1}$$

$$C_m \frac{dT_m}{dt} = K_1(T_s - T_m) + K_0(T_h - T_m) \tag{2}$$

$$T_h = T_{0h} + \beta t, \tag{3}$$

where T_s, T_m and T_h are the sample temperature, temperature at the monitoring station and that at the heat source, respectively. C_s and C_m are the heat capacities of a sample (including the sample pan) and that of the monitoring station, respectively. β is the heating rate which controls T_h. K_0 and K_1 are the heat transfer coefficients between the heat source and the monitoring station, and between the monitoring station and the sample, respectively. This model is schematically presented in Fig. 3. Absorbed or released heat flow rate during the phase transition is represented by F with negative sign for endothermic process.

For the case of melting of pure materials, the above equations are solved for three stages [6,8]. The first stage is before melting ($t < t_{start}$) where the sample temperature T_s increases linearly, the second one is during melting ($t_{start} < t < t_{end}$) where T_s is kept con-

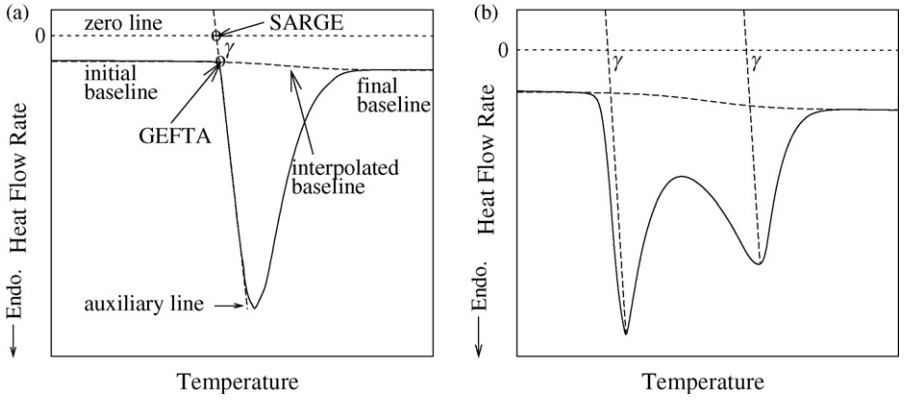

Fig. 2. The definition of extrapolated peak-onset temperatures in GEFTA [9] and SARGE [10] methods. In (a), the temperatures define the melting temperature for a pure material. γ is the slope of the auxiliary line drawn through the descending peak. In (b), the lines at the same slope γ are drawn from the peak tips to assign transition temperatures for a mixture.

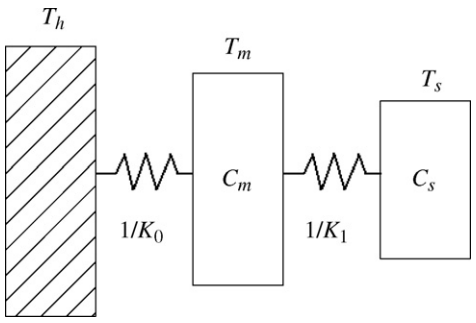

Fig. 3. Schematic representation of the Mraw's model for the sample side where T_h, T_m, and T_s represent, respectively, the temperatures of the heat source, of the monitoring station, and of the sample. C_s is the heat capacity of the sample (plus sample pan) and C_m is that of the monitoring station. K_0 and K_1 are the heat transfer coefficients.

stant, and the last one is after melting ($t_{end} < t$) where T_s returns to the linear increase with a relaxation time depends on instruments. The solutions of Eqs. (1)–(3) for each stage are as follows. For $t < t_{start}$,

$$T_{s1} = T_{0h} + \beta t - \beta\left(\frac{C_s}{K_1} + \frac{C_s + C_m}{K_0}\right) \tag{4}$$

$$T_{m1} = T_{0h} + \beta t - \beta\frac{C_s + C_m}{K_0}. \tag{5}$$

For $t_{start} < t < t_{end}$,

$$T_{s2} = T_M = T_{0h} + \beta t_{start} - \beta\left(\frac{C_s}{K_1} + \frac{C_s + C_m}{K_0}\right) \tag{6}$$

$$T_{m2} = T_M + \beta\frac{C_s}{K_1} + \alpha\Delta t_2 + \frac{K_1}{(K_0 + K_1)^2}\beta C_m \times \left\{1 - \exp\left(-\frac{K_0 + K_1}{C_m}\Delta t_2\right)\right\} \tag{7}$$

$$\Delta t_2 \equiv t - t_{start} \tag{8}$$

$$\alpha \equiv \frac{K_0}{K_0 + K_1}\beta, \tag{9}$$

where T_M represents the melting point and α represents the effective heating rate on the second stage. For $t_{end} < t$,

$$T_{s3} = T_{0h} + \beta t - \beta\left(\frac{C_s}{K_1} + \frac{C_s + C_m}{K_0}\right) + a_1\exp(-\lambda_1\Delta t_3) + a_2\exp(-\lambda_2\Delta t_3) \tag{10}$$

$$T_{m3} = T_{0h} + \beta t - \beta\left(\frac{C_s + C_m}{K_0}\right) + b_1\exp(-\lambda_1\Delta t_3) + b_2\exp(-\lambda_2\Delta t_3) \tag{11}$$

$$\Delta t_3 \equiv t - t_{end}, \tag{12}$$

where λ_1 and λ_2, the inverse of the apparatus relaxation time, are the solutions of the following equation ($0 < \lambda_1 < \lambda_2$),

$$\lambda^2 - \left(\frac{K_1}{C_s} + \frac{K_1}{C_m} + \frac{K_0}{C_m}\right)\lambda + \frac{K_0K_1}{C_sC_m} = 0. \tag{13}$$

The constants a_1, a_2, b_1 and b_2 are determined by the continuation of T_s and T_m between the successive stages.

2.2. The deconvolution of instrumental effects

Eqs. (1)–(3) represent the balance of heat flow rate in the sample side. The deconvolution method proposed by Toda et al. [8] is therefore for a single calorimeter without concerning the information from the reference side. In Eqs. (1)–(3), we have the time sequence of temperature at the monitoring station of the sample side, (t, T_m). The purpose of the deconvolution is to extract the heat flow rate of transition, F, and the true sample temperature, T_s, from those data set with the pre-determined instrumental coefficients, K_0, K_1, C_m, and the sample (plus sample pan) heat capacity, C_s. The determination methods of those coefficients and C_s are as follows.

Firstly, the coefficient, K_0 can be calculated from the following integration, which corresponds to the enthalpy of fusion, ΔH_{fus}.

$$K_0\left\{\int_{t_{start}}^{t_{end}}(T_{m2} - T_{m0})dt + \int_{t_{end}}^{t_\infty}(T_{m3} - T_{m0})dt\right\} = \Delta H_{fus}. \tag{14}$$

Here, T_{m0} is the temperature at the monitoring station in the case of no heat flow rate F of the phase transition, thus the temperature has the same function form with Eq. (5) but is still affected by the change of C_s due to the phase transition. T_{m0} is obtained by fitting T_m in $t < t_{start}$ and $t_{end} \ll t$ and interpolating between the two in the region of transition, $t_{start} < t < t_{end}$. To obtain K_0 using Eq. (14), one can use a standard material such as water. Secondly, the coefficient, K_1 is determined using Eq. (9)

$$K_1 = K_0\left(\frac{\beta}{\alpha} - 1\right) \tag{15}$$

with experimentally obtained α. Then, the coefficient, C_m is calculated by

$$C_m = \frac{K_0}{\lambda} + \frac{K_1}{\lambda - K_1/C_s} \tag{16}$$

using the experimentally measured value of λ and C_s. Here, C_s is determined by

$$C_s = -\frac{\dot{Q}_0}{\beta} \tag{17}$$

where the heat flow rate $\dot{Q}_0$ represents the one without F.

Using the instrumental coefficients and C_s thus obtained, the time sequence of sample temperature T_s and the heat flow rate of the phase transition F are calculated. From Eqs. (2), (3) and (5), the sample temperature T_s is given by

$$T_s = T_m + \frac{1}{K_1}\left[C_m\left(\frac{dT_m}{dt} - \beta\right) - K_0(T_{m0} - T_m) - \beta C_s\right]. \tag{18}$$

The heat flow rate F is obtained from Eq. (1) as

$$F = -K_1(T_m - T_s) + C_s\frac{dT_s}{dt}. \tag{19}$$

3. Experimental

A DSC 2920 Module controlled with Thermal Analyst 2200 (TA Instruments) was used for all measurements. The cell was purged with nitrogen gas with a flow rate 40 ml min^{-1}. Reference pan was removed in all the experiments [12].

Melting behaviors of pure ice were examined at the heating rates of $\beta = 0.2$–10 K min^{-1}. The aqueous solutions with different concentrations of NaCl and glycerol were prepared at room temperature. About 10 mg samples of each solution were sealed hermetically into aluminum pans. The temperature was scanned from the room temperature to 40 °C with a heating rate $\beta =$ 5 K min^{-1} and then kept there for 2 min. The second scan with the same heating rate from −50 to 40 °C followed a cooling run at a rate of 1 K min^{-1}. Water evaporation was checked by measuring

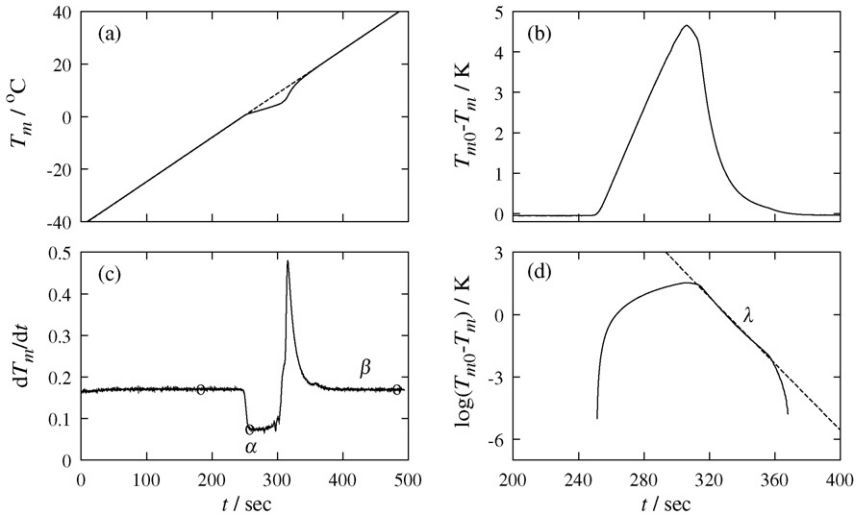

Fig. 4. Temperature at the monitoring station T_m for pure water: (a) the raw data (solid line) and T_{m0} (dashed line), (b) $T_{m0} - T_m$, (c) the time derivative of T_m from which α and β are determined, and (d) the logarithmic plot of (b), from which the slope λ is determined.

the sample weight before and after the experiment. The lost weight was less than 0.1%.

4. Results and discussion

4.1. Determination of the instrumental coefficients

In this section we explain the procedure to determine the instrumental coefficients K_0, K_1, and C_m necessary to construct the true sample temperature T_s and heat flow rate F. As our aim was to construct phase diagrams of aqueous solution, we have chosen pure water as a standard material. Since the instrumental effects become more serious as the heating rate is increased, the data taken at the highest heating rate (10 K min^{-1}) was used.

Figs. 4 and 5 show the obtained data [Figs. 4(a) and 5(a)] during melting of the pure ice and their analysis [Figs. 4(b)–(d) and 5(b)]. Fig. 4(b) shows the temperature change due to the phase transition, $T_{m0} - T_m$, whose integration gives ΔH_{fus} according to Eq. (14). We used the value of ΔH_{fus} of pure ice, 6.0 kJ mol^{-1} to calculate K_0.

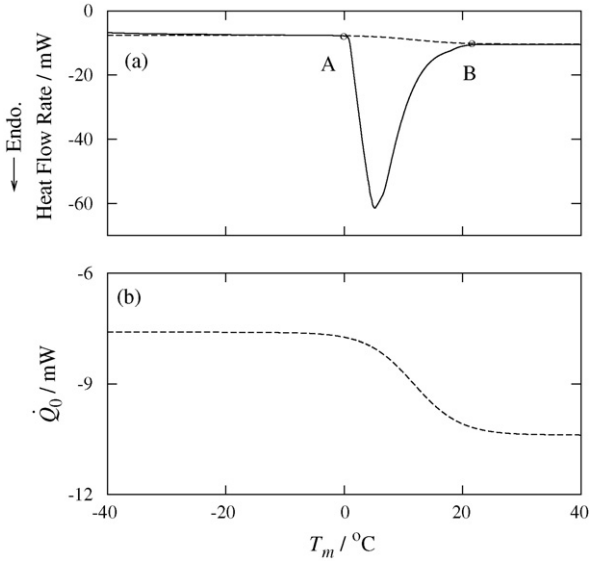

Fig. 5. (a) Heat flow rate from pure water (solid line) and the baseline $\dot{Q}_0$ (dashed line) fitted by a sigmoidal curve shown in (b).

The effective heating rate during the phase transition, α, and the heating rate β before and after the transition were measured as shown in Fig. 4(c). For β we have used the average value. Then using Eq. (15) and the obtained values, we determined K_1.

Now we discuss the determination process of C_m from λ and C_s, using Eq. (16). Firstly, from the slope shown in Fig. 4(d) λ is determined. Secondly, before going to determine C_s, $\dot{Q}_0$ was determined with the fitting of the heat flow rate data using a sigmoidal function as shown in Fig. 5(a). Using the obtained $\dot{Q}_0$ shown in Fig. 5(b), we determined C_s according to Eq. (17). As shown in Fig. 5(b), $\dot{Q}_0$, thus C_s, depends on T_m. To determine C_m, we used a C_s averaged over the transition region. All those obtained coefficients are listed in Table 1. With the obtained instrumental coefficients, it is now possible to deconvolute an experimental thermogram to extract true one.

Fig. 6 shows the melting behaviors of pure ice measured with different heating rates. The raw thermograms and the corresponding deconvoluted ones are respectively shown in Fig. 6(a) and (b). After the deconvolution, the melting peaks shifted toward left side with almost the same onset temperature. The slight peaks seen just after the main peaks in Fig. 6(b) are artifacts resulted from the deconvolution. The peak and onset points are plotted against β in Fig. 6(c). Whereas the peak and onset points of the raw thermograms increased with β, the increase was significantly suppressed after the deconvolution. Especially, the onset points of the deconvoluted data were almost independent of β with a slight increase of less than 0.03 °C. This shows the effectiveness of the deconvolution and confirms that the instrumental coefficients do not depend much on the heating rate. In the next section, we applied the method to the eutectic mixtures of aqueous solution through the construction of phase diagrams.

4.2. Applications

Thermograms of aqueous NaCl and glycerol solutions measured by CDSC-HF are shown in Fig. 7. It is noted that, in Fig. 7(c) and

Table 1
The instrumental coefficients determined experimentally with β=10 K min^{-1}. C_s is the averaged value.

K_0/mW K^{-1}	K_1/mW K^{-1}	λ/s^{-1}	C_m/mJ K^{-1}	C_s/mJ K^{-1}
11.2	14.9	0.08	69.0	51.4

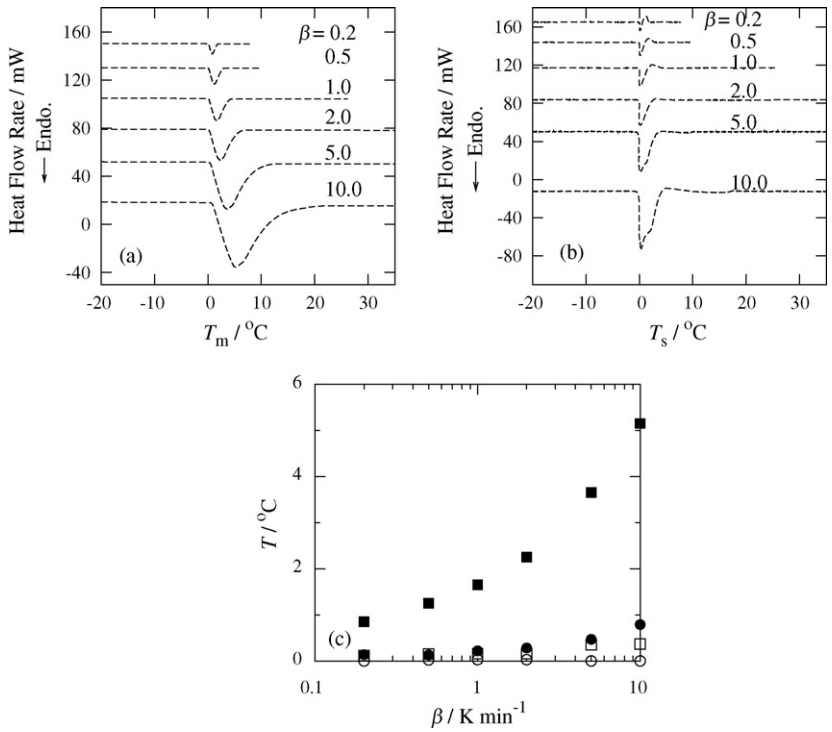

Fig. 6. Heating rate effects on the melting behaviors of pure ice: (a) the raw data, (b) the corresponding results of the deconvolution, and (c) the peak and onset temperatures obtained from the thermograms. In (c), squares and circles, respectively represent the peak and onset temperatures. Filled symbols are from the raw thermograms in (a), and open ones are from the deconvoluted thermograms in (b). In (a) and (b), the heat flow rates are shifted in the *y*-axis direction to show the thermograms at all heating rates.

(d), the first (eutectic) peak was not observed due to the slow crystallization rate of the glycerol. For the deconvolution of the thermograms, we have utilized the same instrumental coefficients listed in Table 1, determined by the measurements of pure water. After the deconvolution the peaks were shifted toward left side with the reduction of the peak width. The sharpness of the peak, which enhances the resolution of peak detection, is important for the study of mixtures which often exhibit two or more close or overlapping melting peaks. Moreover, the deconvolution gives more accurate estimation of the peak area.

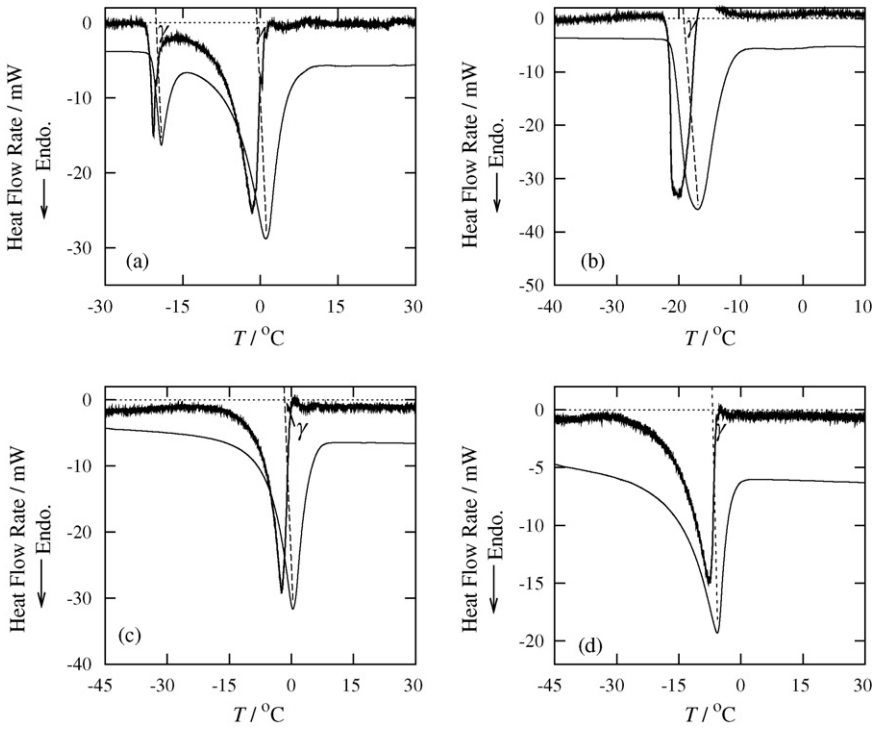

Fig. 7. Thermograms in the melting region of the aqueous solutions of (a) NaCl 4 wt%, (b) NaCl 23.3 wt% at the eutectic composition, (c) glycerol 10 wt%, and (d) glycerol 25 wt%. The raw thermogram and the corresponding deconvoluted thermogram (heat flow rate of transition *F*) are shown by the thin and thick solid curves, respectively. The broken lines represent the extrapolation with the slope γ taken from the thermogram of pure ice.

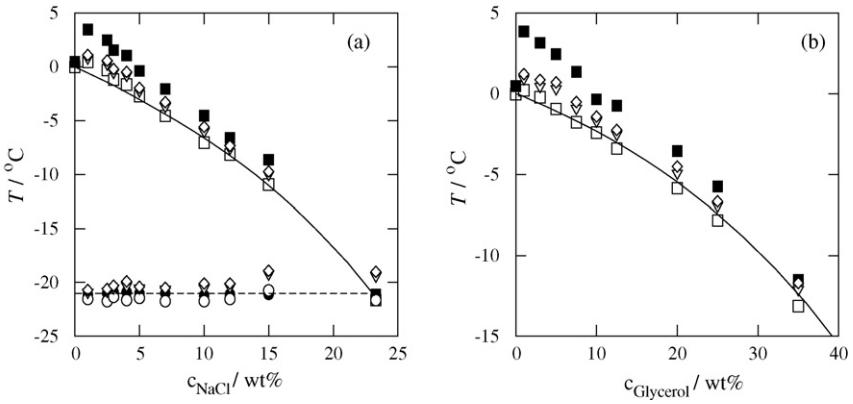

Fig. 8. The phase behaviors of the aqueous solutions of (a) NaCl and (b) glycerol. Open squares and circles represent ice (liquidus) and eutectic (solidus) melting temperatures determined with the deconvolution, and the filled squares and circles are those from raw thermograms. Downward-triangles and diamonds represent those estimated from the SARGE and GEFTA methods, respectively. The solid and dashed curves represent the melting points in the literature [13–15].

Fig. 8 shows the phase diagrams of NaCl and glycerol aqueous solutions, where the solid and dashed curves represent the known melting points [13–15]. To construct the phase diagrams, we chose the onset temperatures for pure ice, for NaCl solution at the eutectic composition (23.3 wt%), and for the first peak at the eutectic temperature of the solutions. This choice is due to the fact that the temperature during the phase transition is kept constant for pure materials or for mixtures at the eutectic point. On the other hand, the liquidus temperatures correspond to the ending temperatures of the melting of the eutectic mixtures [the second peak in Fig. 7(a) and the peaks in Fig. 7(c) and (d)]. For the temperatures, we used the peak temperature because there still seemed to remain a weak influence of the instrumental effects as a tail of the peak. With the combination of these choices, the melting points determined agreed well with the reported data as shown in Fig. 8. On the other hand, the peak temperatures of the raw data and the extrapolated onset temperatures estimated from GEFTA and SARGE methods were located at slightly higher temperatures than the true values as shown in Fig. 8. It should also be noted that, for the ending temperature of the melting at the liquidus temperature, the extrapolation of the second peak to the "onset" temperature in GEFTA and SARGE methods is not on physically reasonable basis. Thus present results clearly demonstrate the applicability of the deconvolution method for the study of the phase behaviors in eutectic mixtures. It can also be said that, for the sample mass of *ca.* 10 mg in the present experiments, the effects of temperature gradient in the sample were negligible in comparison with the instrumental effects. It is noted that, in Fig. 8, a slight increase (less than 0.3 K) of liquidus temperature from the literature value is recognized for solutions at concentrations less than 3 wt%, while the melting temperature of pure ice at 0 wt% was in good agreement. As mentioned above, for the melting of ice in the mixture, we chose the peak temperature of the deconvoluted heat flow rate, while for pure ice, the onset temperature of the peak. Therefore, this deviation can be the indication of somehow insufficient deconvolution of the instrumental effects for the ending of the second peak with relatively larger melting peak of ice at low concentrations of NaCl and glycerol.

5. Conclusions

A deconvolution method on conventional DSC was reviewed and applied on the phase transition in eutectic mixtures through the construction of the phase diagrams. With the deconvolution, melting points were measured accurately even at the heating rate as high as 10 K min^{-1}. The method was applied on the construction of phase diagrams of aqueous mixtures where the accurate interpretation of the peak profile was essential. The agreement between obtained phase diagrams and those in the literature suggests the applicability of the method for the study of phase transitions in eutectic mixtures.

Acknowledgments

The authors wish to thank Prof. K. Taguchi and Dr. H. Kajioka of Hiroshima University for helpful discussions. This work was supported by KAKENHI (Grant-in-Aid for Scientific Research) on Priority Area "Soft Matter Physics" from the Ministry of Education, Culture, Sports, Science and Technology of Japan.

References

[1] J. Jin, M. Song, F. Pan, Thermochim. Acta 456 (2007) 25–31.
[2] J. Jin, M. Song, Thermochim. Acta 438 (2005) 95–101.
[3] K. Yukimitu, R.C. Oliveira, E.B. Araujo, J.C.S. Moraes, L.H. Avanci, Thermochim. Acta 426 (2005) 157–161.
[4] W.J. Boettinger, U.R. Kattner, K. Moon, J.H. Perepzko, in: J.-C. Zhao (Ed.), DTA and Heat-Flux DSC Measurements of Alloy Melting and Freezing, Elsevier, UK, 2007, chapter 5.
[5] S.C. Mraw, Rev. Sci. Instrum. 53 (1982) 228–231.
[6] Y. Saito, K. Saito, T. Atake, Thermochim. Acta 99 (1986) 299–307.
[7] R.L. Danely, Thermochim. Acta 395 (2003) 201–208.
[8] A. Toda, M. Hikosaka, K. Yamada, Polymer 43 (2002) 1667–1679.
[9] G.W.H. Hohne, H.K. Cammenga, W. Eysel, E. Gmelin, W. Hemminger, Thermochim. Acta 160 (1990) 1–12.
[10] S.M. Sarge, Thermochim. Acta 187 (1991) 323–334.
[11] R.C. Gosh, A. Toda, S. Tanaka, Polymer 50 (2009) 1304–1310.
[12] I. Hatta, S. Muramatsu, Jpn. J. Appl. Phys. 35 (1996) L858–L860.
[13] A.V. Wolf, G.M. Brown, G.P. Prentiss, in: R.C. Weast (Ed.) Concentrative Properties of Aqueous Solutions: Conversion Tables, CRC Press Inc., Boca Raton, FL, 1989–1990, D-234.
[14] D.L. Hall, S.M. Sterner, R.J. Bodnar, Econ. Geol. 83 (1988) 197–202.
[15] B. Han, J.H. Choi, J.A. Dantzig, J.C. Bischof, Cryobiology 52 (2006) 146–151.